CHEMICAL PHYSICS

A reversible single-molecule switch based on activated antiaromaticity

Xiaodong Yin,[1]* Yaping Zang,[2]* Liangliang Zhu,[3]* Jonathan Z. Low,[1] Zhen-Fei Liu,[4] Jing Cui,[2] Jeffrey B. Neaton,[4†] Latha Venkataraman,[1,2†] Luis M. Campos[1†]

Single-molecule electronic devices provide researchers with an unprecedented ability to relate novel physical phenomena to molecular chemical structures. Typically, conjugated aromatic molecular backbones are relied upon to create electronic devices, where the aromaticity of the building blocks is used to enhance conductivity. We capitalize on the classical physical organic chemistry concept of Hückel antiaromaticity by demonstrating a single-molecule switch that exhibits low conductance in the neutral state and, upon electrochemical oxidation, reversibly switches to an antiaromatic high-conducting structure. We form single-molecule devices using the scanning tunneling microscope–based break-junction technique and observe an on/off ratio of ~70 for a thiophenylidene derivative that switches to an antiaromatic state with 6-4-6-π electrons. Through supporting nuclear magnetic resonance measurements, we show that the doubly oxidized core has antiaromatic character and we use density functional theory calculations to rationalize the origin of the high-conductance state for the oxidized single-molecule junction. Together, our work demonstrates how the concept of antiaromaticity can be exploited to create single-molecule devices that are highly conducting.

INTRODUCTION

The ability to miniaturize macroscopic devices and electronic components at the molecular level provides unprecedented fundamental information on chemical structure and, importantly, bridges the gap toward single-molecule devices (*1*–*4*). Although the concept for a molecular rectifier was proposed in 1974 (*5*), recent breakthroughs, which stem from advanced nanofabrication and device characterization techniques, have led to the observation of thermoelectric behavior (*6*), the Kondo effect (*7*, *8*), rectification (*9*), and switching (*10*–*14*). These advances have been due, in part, to the ability to use different aromatic molecular components as the functional elements of the devices. Surprisingly, structures that focus on Hückel antiaromaticity, a classical physical organic chemistry concept, have been overlooked. Although it has been shown that the aromatic character of a molecular component can control conductance, the concept of antiaromaticity has not been successfully implemented in molecular switches, because antiaromatic compounds are generally unstable (*15*).

Herein, we designed an electrochemically activated redox-active molecular wire that is based on the thieno derivative [8,8′-biindeno[2,1-*b*] thiophenylidene (**BTP**)] (*16*) of 9,9′-bifluorenylidene (Fig. 1) (*17*). These systems are known to be efficient electron acceptors, because upon reduction, they gain 6-6-6-π electron aromaticity. The important feature that we exploit is oxidation to the 6-4-6-π electron antiaromatic central rings, which does not involve making or breaking σ bonds, as in the case of most commonly studied switching mechanisms (*10*, *18*, *19*). Upon oxidation, the central ring of the **BTP** system takes on antiaromatic characteristics with 4π electrons. Because antiaromatic systems are known to be unstable, the carbocycles flanking the central ring delocalize the charge and provide stability (*20*, *21*). To form single-molecule junctions to investigate the charge transport properties of the parent **BTP** core, we added thiochroman linkers (*22*), yielding the structure shown in Fig. 2A [thiochromatin derivative of BTP (**TBTP**)]. Synthetic and molecular characterization details are given in the Supplementary Materials.

RESULTS AND DISCUSSION

We first characterize the solution-based optical and electronic properties of the **TBTP** by cyclic voltammetry (CV) and spectroelectrochemistry. Figure 2B shows a CV plot where we see four reversible redox peaks, two corresponding to oxidation and two corresponding to reduction. We note that the two oxidation peaks at E_{ox1} = 0.41 V and E_{ox2} = 0.56 V (versus ferrocene [$Fc^{+/0}$]) are close in energy, whereas the reduction peaks are well separated. To characterize the changes in optical properties of **TBTP** under various applied electrochemical potentials, we measure ultraviolet–visible (UV-vis) absorption spectra of **TBTP** at different potentials. We start with the neutral molecule that exhibits an optical energy gap of 1.77 eV (fig. S1). Upon applying a potential of 0.9 V (versus ferrocene [$Fc^{+/0}$]), the molecule is doubly oxidized (+2 state), and the optical gap decreases to about 0.85 eV (Fig. 2C). The spectroelectrochemical changes are reversible, as is visible from the CV and additional UV-vis spectra (fig. S2), which shows the spectral characteristics of the transient radical cation. To probe changes to the molecular structure after oxidation, we chemically oxidize **TBTP** with $AgSbF_6/I_2$, and this shows further evidence of the +2 state by matching the UV-vis spectra to the spectroelectrochemistry data (the radical cation is not observed by chemical oxidation). **TBTP** can be chemically oxidized reversibly (fig. S3), and the dication exhibits remarkable stability at ambient conditions for several hours. Considering that the antiaromaticity of this stable system can be probed by proton nuclear magnetic resonance (^{1}H-NMR) (*23*), we collected the ^{1}H-NMR spectra for the neutral and chemically oxidized **TBTP** at room temperature. The NMR spectra show that the proton signal from the benzene ring of the **BTP** core exhibits a marked upshielding shift, indicating antiaromatic character (fig. S4). Although this upshielding shift is not seen for all protons on the core due to charge delocalization, this key result is

[1]Department of Chemistry, Columbia University, New York, NY 10027, USA. [2]Department of Applied Physics, Columbia University, New York, NY 10027, USA. [3]State Key Laboratory of Molecular Engineering of Polymers, Department of Macromolecular Science, Fudan University, Shanghai 200433, China. [4]Molecular Foundry, Lawrence Berkeley National Laboratory, and Department of Physics, University of California, Berkeley, Berkeley, CA 94720, USA.
*These authors contributed equally to this work.
†Corresponding author. Email: lv2117@columbia.edu (L.V.); jbneaton@lbl.gov (J.B.N.); lcampos@columbia.edu (L.M.C.)

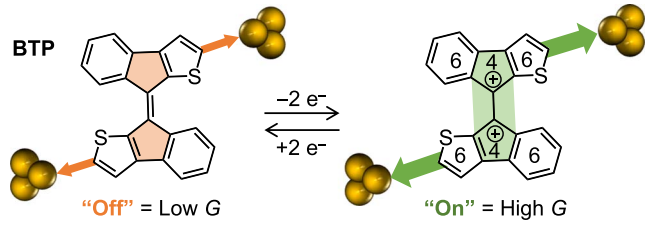

Fig. 1. Model of the electrochemically activated BTP switch. BTP shows the neutral, low-conductance state. Upon oxidation, **BTP** gains antiaromatic character to the 6-4-6-π electron state that exhibits high conductance.

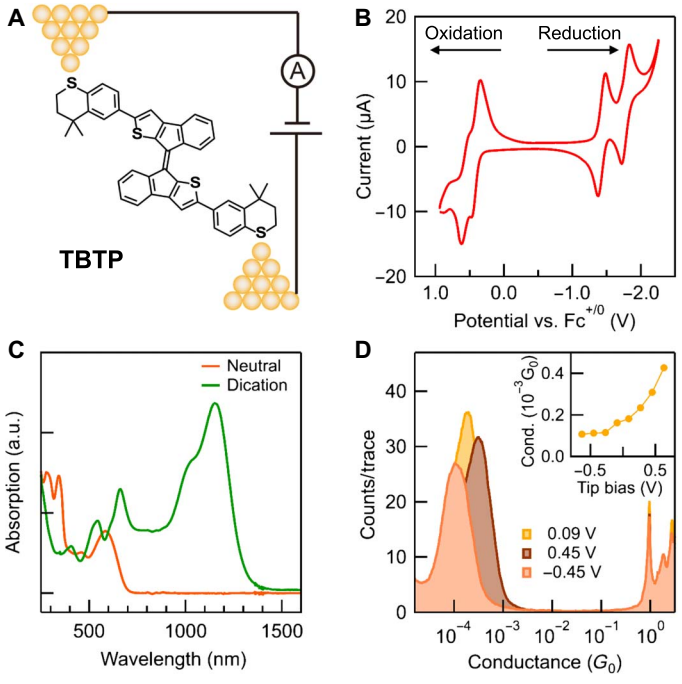

Fig. 2. STM-BJ measurements and electrochemical characterizations of TBTP. (**A**) A schematic diagram of a single Au-**TBTP**-Au junction. (**B**) Cyclic voltammogram of **TBTP** in dichloromethane solution (1 mM) with Bu_4NPF_6 (0.1 M) as the supporting electrolyte. Scan rate used is 100 mV/s. (**C**) Steady-state linear absorption spectroscopy of the neutral **TBTP** (orange) and the dication (green) obtained at a potential of 0.9 V (versus ferrocene [$Fc^{+/0}$]). a.u., absorbance units. (**D**) Logarithm-binned 1D histograms (100 bins/decade) for **TBTP** in PC with tetrabutylammonium perchlorate at a tip bias of 0.09, 0.45, and −0.45 V (tip relative to the substrate). Inset: Peak conductance value versus applied tip bias.

consistent with the NMR spectra predicted by density functional theory (DFT) calculations, as detailed in Materials and Methods. Thus, it can be concluded that the **BTP** core takes on antiaromatic character in the +2 state, consistent with the simple electron-counting picture presented above.

To test the hypothesis that antiaromaticity can lead to highly conductive molecular devices, we performed single-molecule measurements under an electrochemical potential using the scanning tunneling microscope break-junction (STM-BJ) technique (*24*, *25*). The details of the method have been described before by Capozzi *et al.* (*24*). Briefly, we use a gold STM tip and substrate, which forms the working electrodes, whereas an additional Pt wire introduced into the fluid cell serves as the counter (or gate) electrode. Measurements are carried out in 0.1 mM **TBTP** solution in propylene carbonate (PC), a polar solvent, with 0.1 M tetrabutylammonium perchlorate as the supporting electrolyte, and potential calibrations are carried out by adding ferrocene to the solution and measuring its reversible oxidation potential. The tip is insulated with Apiezon wax to reduce the background ionic current (*26*). The conductance of **TBTP** is first measured without applying a gate voltage. Figure 2D shows the one-dimensional (1D) conductance histograms of **TBTP** at a tip bias of 0.09, 0.45, and −0.45 V relative to the substrate. Each conductance histogram reveals a clear narrow peak at a bias-dependent conductance value. The inset of Fig. 2D shows the peak conductance plotted against the tip bias (see fig. S5 for full data sets), where a modest conductance increase of a factor of 5 is seen within this bias range. Such a bias polarity–dependent conductance indicates that the highest occupied molecular orbital (HOMO) dominates charge transport (*27*).

The electrochemical switching of the single-molecule junction was accomplished by changing the voltage applied to the Pt gate electrode (relative to the substrate) and repeating the measurements while maintaining a low bias voltage of 25 mV on the tip (also relative to the substrate). Note that in this STM-BJ measurement, the voltage is applied to the gate electrode, relative to the substrate. Therefore, oxidation events are observed at negative gate voltages. This is corroborated by the in situ electrochemistry shown in fig. S6A. By contrast, in traditional CV measurements, the potential is applied to the working electrode, relative to the reference. Conductance histograms measured at different voltages applied to the gate are shown in Fig. 3A. At the positive gate voltage, the conductance peak shifts to lower values, consistent with transport being dominated by the HOMO. At negative gate voltages, a modest increase of the conductance is first observed until an applied gate voltage of about −1.4 V (+1 V measured potential relative to $Fc^{+/0}$). Beyond −1.4 V, the conductance peak shifts markedly by a factor of ~70 (Fig. 3A), and the histograms broaden—an aspect we will discuss further below. This sharp increase in conductance is visible in the inset of Fig. 3A, where we plot the measured conductance against the gate potential (see fig. S5B for full data sets). We show further that the switching is reversible by changing the gate potential between negative (<−1.5 V) and positive (>1 V) values, in an alternating fashion, after every 100 conductance traces. The conductance peak values determined from the histogram of these traces (fig. S6B) are plotted in Fig. 3B, yielding an average on/off ratio value of ~70. Note that the redox-switching experiments were conducted at ambient conditions, without the rigorous exclusion of air and moisture. In addition, to show that the gate potential does change the oxidation state of the molecules in solution in our STM setup, we record the in situ linear sweep voltammetry (LSV), measuring the current through the STM tip as a function of the applied gate voltage. We do this measurement after adding ferrocene to the solution to calibrate the applied gate voltage and confirm oxidation states (fig. S6A). We see a broad oxidation peak at a gate voltage of −1.4 V, consistent with our finding that a negative gate voltage needs to be applied to measure the conductance of the oxidized **TBTP**.

To confirm that we are measuring the conductance of a **TBTP** molecule bridging the gap between two Au electrodes, we compare 2D conductance-displacement histograms compiled from these data in Fig. 3 (C and D) (*28*). Both figures show a molecular feature that extends by about 1 nm relative to the point where the gold point contact is ruptured. We have previously shown that the extent of the 2D histogram feature relates to the molecular backbone length (*28*), and thus, these data reveal that a stable molecular junction is formed at the high negative gate bias. The key result of this study is that changing the oxidation state of **TBTP** without making/breaking covalent bonds results

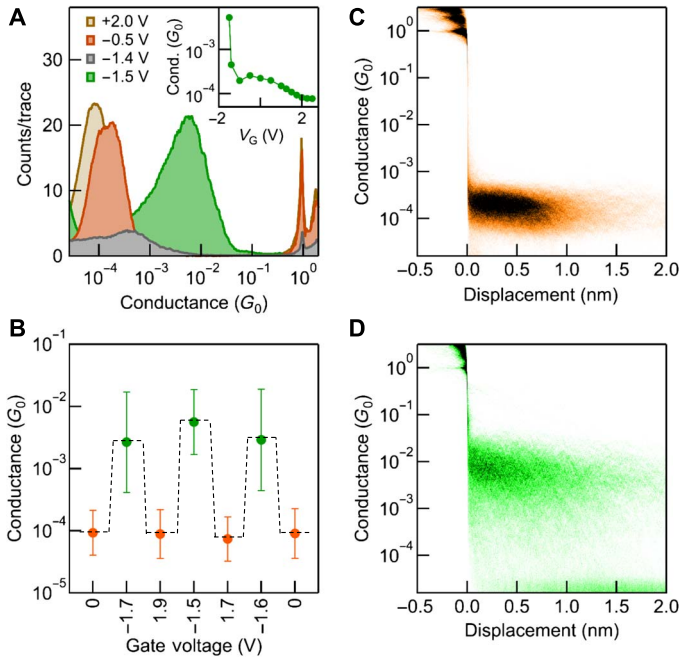

Fig. 3. STM-BJ results showing the reversible single-molecule switch. (**A**) Logarithm-binned 1D histograms for **TBTP** in PC with tetrabutylammonium perchlorate as the supporting electrolyte at a gate voltage (V_G) of +2, −0.5, −1.4, and −1.5 V. The gate voltage is applied relative to the substrate. Inset: Peak conductance value versus applied gate voltage. (**B**) Cyclic on/off conductance values determined by switching between the positive gate voltage and negative gate voltage chosen to be beyond the oxidation/reduction thresholds. Error bars correspond to the full width at half maximum of the conductance histogram peaks. (**C** and **D**) 2D conductance-displacement histogram for **TBTP** at off state (V_G = 0 V) (C) and on state (V_G = −1.5 V) (D). Note that the bias applied across the molecular junction is fixed at 25 mV (tip relative to the substrate) during these measurements.

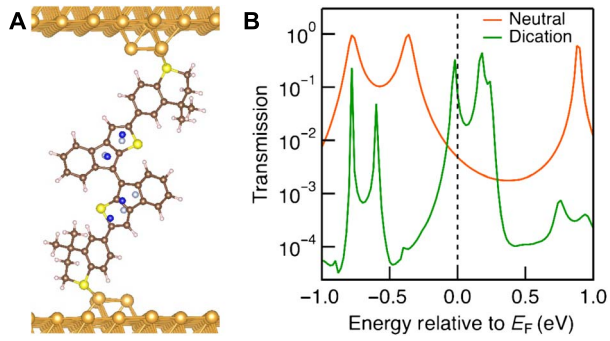

Fig. 4. DFT-based transmission calculations. (**A**) The molecular junction containing the neutral **TBTP** molecule (H, light pink; C, brown; and S, yellow) and eight fluorine atoms at about 1 Å above (dark blue) and below (light blue) the central rings to model the **TBTP** molecule in a +2 oxidized state. (**B**) Transmission as a function of energy for the neutral (orange) and the oxidized molecule (green). E_F is the Fermi level of the junction.

in a large change in conductance, which can be attributed to the increased antiaromatic character of the oxidized species.

To provide further support for the observed increased conductance upon oxidation, we turn to DFT-based calculations of the single-molecule junction. We first construct the molecular junction containing the neutral **TBTP** (see Fig. 4A for the geometry) and perform conductance calculations with a DFT-based nonequilibrium Green's function (NEGF) approach, with the TranSIESTA package (see Materials and Methods for details) (*29*). Figure 4B shows the resulting transmission as a function of energy (orange trace). The conductance at zero bias (transmission at Fermi energy) is small and corresponds to a junction in its "off" state. We note that for a quantitative comparison between theory and experiment, self-energy corrections to the DFT mean-field eigensystem are required, as in, for example, the approximate DFT + Σ method (see Materials and Methods and the Supplementary Materials) (*30*). Here, we focus on the comparison between the neutral and the oxidized **TBTP** molecule. To model the molecule in a +2 oxidation state, eight fluorine atoms are added around the **BTP** core at approximately 1 Å above and below the central rings, such that the total Mulliken charge on the molecule reaches +2 in the gas phase (see Fig. 4A for the geometry). We then perform a DFT-NEGF calculation of the molecular junction with the fluorine atoms present. The resulting transmission is shown in Fig. 4B.

The transmission functions of both the neutral and oxidized species show stark differences. The oxidized **TBTP** leads to a partially occupied resonance and much higher transmission close to the Fermi energy. This increase corresponds to a conductance enhancement of a factor of ~60, consistent with the experimental results, where the average on/off ratio is ~70. Although the actual conductance of the oxidized species may be sensitive to the parameters of the calculation, the qualitative trend of increasing conductance after oxidization is correctly captured here. Because the resonance close to the Fermi level is quite narrow, small changes in the metal work function as a result of changes in junction geometry or ionic environment could result in large changes in conductance. This is consistent with the experimental data that shows a broader conductance peak for the +2 state of **TBTP**.

MATERIALS AND METHODS

Molecular characterizations

^{1}H-NMR and ^{13}C-NMR were recorded on a Bruker Avance III 500 (500 MHz) spectrometer in dichloromethane-d_2 [residual solvent peak at δ = 5.32 parts per million (ppm) for ^{1}H NMR] and chloroform-*d* solution (residual solvent peak at δ = 77.16 ppm for ^{13}C NMR). Mass spectra were obtained at the Columbia University Mass Spectrometry Facility using a Xevo G2-XS (Waters) equipped with a quadrupole time-of-flight detector with multiple inlet and ionization capabilities, including electrospray ionization, atmospheric pressure chemical ionization, and atmospheric solids analysis probe. The base peaks were usually obtained as $[M]^+$ or $[M + H]^+$ ions. UV-vis absorption data were acquired on a Varian Cary 5000 UV-Vis-NIR spectrophotometer. Cyclic voltammograms were recorded on a CHI 66 electrochemical workstation using Pt plate electrode as the working electrode, Pt wire as the counter electrode, and Ag/AgCl electrode as the reference electrode at room temperature.

STM-BJ measurements

Conductance measurements were performed using a custom STM that has been described in detail before (*31*). Conductance measurements were performed in dilute solutions (10 to 100 μM) in PC with tetrabutylammonium perchlorate as the supporting electrolyte. The insulated tips were created by driving a mechanically cut gold tip through Apiezon wax (*26*). 1D conductance histograms were constructed using

logarithmic bins (100 bins/decade), and 2D histograms used logarithmic bins along the conductance axis (100 bins/decade) and linear bins along the displacement axis. All histograms were constructed without any data selection.

Antiaromaticity characterizations

To characterize the antiaromatic character of the oxidized **TBTP**$^{2+}$, the NMR spectra of the neutral and oxidized species were collected at room temperature (*23*). The oxidant, $AgSbF_6/I_2$, was added to the solution of **TBTP** in deuterated dichloromethane (CD_2Cl_2) in a 2:1 ratio (oxidant/**TBTP**) (*32*).

Calculation of the NMR spectra and nuclear-independent chemical shifts

We calculated the NMR spectra and nuclear-independent chemical shift (NICS) using DFT within the Gaussian 09 suite (*33*). All geometries were optimized with B3LYP functional and the 6-31G** basis set. NMR and NICS calculations were conducted with the GIAO-B3LYP/6-31G** method. The calculated NMR chemical shifts are generally consistent with the experimental ones as indicated in table S1. The change of aromaticity for all the rings in the **BTP** core can be determined from NICS calculations. In general, a positive NICS value indicates an antiaromatic character, whereas a negative NICS value indicates aromatic character (*34*, *35*). We calculated two types of NICS values: NICS(1)_zz, which represents the NICS 1 Å above and below center mass of the ring, and NICS(0), which gives NICS value at the center of mass of the ring. Results are reported in table S2.

Transport calculations

We relaxed the junction geometry using the Perdew-Burke-Ernzerhof (PBE) functional (*36*), as implemented in SIESTA package (*37*). Pseudopotentials and basis sets were adapted from a previous work (*30*). Each electrode consisted of seven layers of 36 gold atoms forming a 6×6 unit cell of the Au(111) surface. In addition, the S atoms in the molecule were attached to the gold substrate using trimer binding motifs. During geometry relaxation, the outer four layers of gold on each side were treated as a "rigid body" and were only allowed to relax along the transport (z) direction, as x and y coordinates were held fixed and the internal atomic distances within this set of gold atoms were kept at bulk values. All x, y, and z coordinates of the molecule, the trimer tip motif, and the inner three layers of gold atoms on each side were allowed to fully relax. In this way, we achieved the optimal geometry around the molecule-gold contact while maintaining the bulk gold geometry far away from the molecule. Periodic boundary conditions with large vacuum along the z direction and a $3 \times 3 \times 1$ k-mesh were used in the geometry relaxation, which was performed until all forces were <0.04 eV/Å. After the junction was relaxed, transport properties were calculated using the TranSIESTA package (*29*) with the same functional, pseudopotentials, basis sets, and k-mesh as above.

It is known that the standard DFT-NEGF formalism overestimates the zero-bias conductance due to underestimation of the level alignment between frontier orbitals of the molecule and the Fermi level of the junction (*30*), especially when local or semilocal functionals are used. We used the DFT + Σ method (*30*, *38*) to correct the level alignment and transport properties. The correction to level alignment consists of two terms: a self-energy correction to the gas-phase HOMO-LUMO (lowest unoccupied molecular orbital) gap and a correction to the electron addition/removal energies due to the electrostatic polarization (image charge) of the electrodes and environment. For the gas-phase correction, we used the optimally tuned range-separated hybrid functional (*39*) to accurately calculate the HOMO energy of the gas-phase molecule. For the **TBTP** molecule, it is −6.2 eV (optimal Coulomb separation parameter is 0.11 bohr^{-1}), yielding a gas-phase correction to the PBE HOMO of 1.8 eV downward. For the "image-charge" contribution, we used the image plane of 0.9 Å, as determined previously (*40*), which results in an image-charge correction of 0.5 eV. The total self-energy correction for HOMO resonance is then 1.3 eV downward. To model the oxidized molecule, we decorated the region around the **BTP** core with eight fluorine atoms and repeated the transmission calculations. However, we cannot use the DFT + Σ method to calculate the transmission for the molecule-fluorine system due to a strong charge transfer between the molecule and the fluorine atoms.

SUPPLEMENTARY MATERIALS

Supplementary material for this article is available at http://advances.sciencemag.org/cgi/content/full/3/10/eaao2615/DC1

Synthetic details

DFT-optimized coordinates

NMR and mass spectroscopy data

fig. S1. UV-vis spectrum of **TBTP**.

fig. S2. Steady-state linear absorption spectroscopy of **TBTP** obtained in a spectroelectrochemical setup.

fig. S3. Steady-state linear absorption spectroscopy of **TBTP** and chemically oxidized **TBTP** dication.

fig. S4. ^{1}H NMR of the neutral **TBTP** and dication obtained by chemical oxidation.

fig. S5. STM-BJ measurements of **TBTP**.

fig. S6. STM-BJ measurements of a reversible single-molecule switch and in situ LSV.

fig. S7. Transmission calculations for the neutral **TBTP** molecule using standard DFT methods and with DFT + Σ.

table S1. DFT calculation (GIAO-B3LYP/6-31G**) of ^{1}H NMR of **TBTP** and **TBTP**$^{2+}$.

table S2. DFT-based NICS calculations of the aromaticity of rings.

REFERENCES AND NOTES

1. A. H. Flood, J. F. Stoddart, D. W. Steuerman, J. R. Heath, Whence molecular electronics? *Science* **306**, 2055–2056 (2004).
2. A. Nitzan, M. A. Ratner, Electron transport in molecular wire junctions. *Science* **300**, 1384–1389 (2003).
3. T. A. Su, M. Neupane, M. L. Steigerwald, L. Venkataraman, C. Nuckolls, Chemical principles of single-molecule electronics. *Nat. Rev. Mater.* **1**, 16002 (2016).
4. N. J. Tao, Electron transport in molecular junctions. *Nat. Nanotechnol.* **1**, 173–181 (2006).
5. A. Aviram, M. A. Ratner, Molecular rectifiers. *Chem. Phys. Lett.* **29**, 277–283 (1974).
6. P. Reddy, S.-Y. Jang, R. A. Segalman, A. Majumdar, Thermoelectricity in molecular junctions. *Science* **315**, 1568–1571 (2007).
7. J. Park, A. N. Pasupathy, J. I. Goldsmith, C. Chang, Y. Yaish, J. R. Petta, M. Rinkoski, J. P. Sethna, H. D. Abruña, P. L. McEuen, D. C. Ralph, Coulomb blockade and the Kondo effect in single-atom transistors. *Nature* **417**, 722–725 (2002).
8. W. Liang, M. P. Shores, M. Bockrath, J. R. Long, H. Park, Kondo resonance in a single-molecule transistor. *Nature* **417**, 725–729 (2002).
9. B. Capozzi, J. Xia, O. Adak, E. J. Dell, Z.-F. Liu, J. C. Taylor, J. B. Neaton, L. M. Campos, L. Venkataraman, Single-molecule diodes with high rectification ratios through environmental control. *Nat. Nanotechnol.* **10**, 522–527 (2015).
10. P. Liljeroth, J. Repp, G. Meyer, Current-induced hydrogen tautomerization and conductance switching of naphthalocyanine molecules. *Science* **317**, 1203–1206 (2007).
11. D. Dulić, S. J. van der Molen, T. Kudernac, H. T. Jonkman, J. J. D. de Jong, T. N. Bowden, J. van Esch, B. L. Feringa, B. J. van Wees, One-way optoelectronic switching of photochromic molecules on gold. *Phys. Rev. Lett.* **91**, 207402 (2003).
12. S. Y. Quek, M. Kamenetska, M. L. Steigerwald, H. J. Choi, S. G. Louie, M. S. Hybertsen, J. B. Neaton, L. Venkataraman, Mechanically controlled binary conductance switching of a single-molecule junction. *Nat. Nanotechnol.* **4**, 230–234 (2009).
13. H. M. Osorio, S. Catarelli, P. Cea, J. B. G. Gluyas, F. Hartl, S. J. Higgins, E. Leary, P. J. Low, S. Martín, R. J. Nichols, J. Tory, J. Ulstrup, A. Vezzoli, D. C. Milan, Q. Zeng, Electrochemical single-molecule transistors with optimized gate coupling. *J. Am. Chem. Soc.* **137**, 14319–14328 (2015).

14. F. Chen, J. He, C. Nuckolls, T. Roberts, J. E. Klare, S. Lindsay, A molecular switch based on potential-induced changes of oxidation state. *Nano Lett.* **5**, 503–506 (2005).
15. W. Chen, H. Li, J. R. Widawsky, C. Appayee, L. Venkataraman, R. Breslow, Aromaticity decreases single-molecule junction conductance. *J. Am. Chem. Soc.* **136**, 918–920 (2014).
16. C.-Y. Chiu, H. Wang, F. G. Brunetti, F. Wudl, C. J. Hawker, Twisted but conjugated: Building blocks for low bandgap polymers. *Angew. Chem. Int. Ed.* **53**, 3996–4000 (2014).
17. F. G. Brunetti, X. Gong, M. Tong, A. J. Heeger, F. Wudl, Strain and Hückel aromaticity: Driving forces for a promising new generation of electron acceptors in organic electronics. *Angew. Chem. Int. Ed.* **49**, 532–536 (2010).
18. R. Breslow, Antiaromaticity. *Acc. Chem. Res.* **6**, 393–398 (1973).
19. C. Jia, A. Migliore, N. Xin, S. Huang, J. Wang, Q. Yang, S. Wang, H. Chen, D. Wang, B. Feng, Z. Liu, G. Zhang, D.-H. Qu, H. Tian, M. A. Ratner, H. Q. Xu, A. Nitzan, X. Guo, Covalently bonded single-molecule junctions with stable and reversible photoswitched conductivity. *Science* **352**, 1443–1445 (2016).
20. W. C. Lothrop, Biphenylene. *J. Am. Chem. Soc.* **63**, 1187–1191 (1941).
21. S. Schneebeli, M. Kamenetska, F. Foss, H. Vazquez, R. Skouta, M. Hybertsen, L. Venkataraman, R. Breslow, The electrical properties of biphenylenes. *Org. Lett.* **12**, 4114–4117 (2010).
22. Y. S. Park, J. R. Widawsky, M. Kamenetska, M. L. Steigerwald, M. S. Hybertsen, C. Nuckolls, L. Venkataraman, Frustrated rotations in single-molecule junctions. *J. Am. Chem. Soc.* **131**, 10820–10821 (2009).
23. M. D. Peeks, T. D. W. Claridge, H. L. Anderson, Aromatic and antiaromatic ring currents in a molecular nanoring. *Nature* **541**, 200–203 (2017).
24. B. Capozzi, Q. Chen, P. Darancet, M. Kotiuga, M. Buzzeo, J. B. Neaton, C. Nuckolls, L. Venkataraman, Tunable charge transport in single-molecule junctions via electrolytic gating. *Nano Lett.* **14**, 1400–1404 (2014).
25. B. Xu, N. J. Tao, Measurement of single-molecule resistance by repeated formation of molecular junctions. *Science* **301**, 1221–1223 (2003).
26. L. A. Nagahara, T. Thundat, S. M. Lindsay, Preparation and characterization of STM tips for electrochemical studies. *Rev. Sci. Instrum.* **60**, 3128–3130 (1989).
27. B. Capozzi, J. Z. Low, J. Xia, Z.-F. Liu, J. B. Neaton, L. M. Campos, L. Venkataraman, Mapping the transmission functions of single-molecule junctions. *Nano Lett.* **16**, 3949–3954 (2016).
28. M. Kamenetska, M. Koentopp, A. C. Whalley, Y. S. Park, M. L. Steigerwald, C. Nuckolls, M. S. Hybertsen, L. Venkataraman, Formation and evolution of single-molecule junctions. *Phys. Rev. Lett.* **102**, 126803 (2009).
29. M. Brandbyge, J.-L. Mozos, P. Ordejón, J. Taylor, K. Stokbro, Density-functional method for nonequilibrium electron transport. *Phys. Rev. B* **65**, 165401 (2002).
30. S. Y. Quek, L. Venkataraman, H. J. Choi, S. G. Louie, M. S. Hybertsen, J. B. Neaton, Amine–gold linked single-molecule circuits: Experiment and theory. *Nano Lett.* **7**, 3477–3482 (2007).
31. L. Venkataraman, J. E. Klare, C. Nuckolls, M. S. Hybertsen, M. L. Steigerwald, Dependence of single-molecule junction conductance on molecular conformation. *Nature* **442**, 904–907 (2006).
32. J. L. Malandra, N. S. Mills, D. E. Kadlecek, J. A. Lowery, Dications of tetrabenzofulvalenes. Paratropicity and σ donation in perpendicular antiaromatic systems. *J. Am. Chem. Soc.* **116**, 11622–11623 (1994).
33. M. J. Frisch, G. W. Trucks, H. B. Schlegel, G. E. Scuseria, M. A. Robb, J. R. Cheeseman, G. Scalmani, V. Barone, B. Mennucci, G. A. Petersson, H. Nakatsuji, M. Caricato, X. Li, H. P. Hratchian, A. F. Izmaylov, J. Bloino, G. Zheng, J. L. Sonnenberg, M. Hada, M. Ehara, K. Toyota, R. Fukuda, J. Hasegawa, M. Ishida, T. Nakajima, Y. Honda, O. Kitao, H. Nakai, T. Vreven, J. A. Montgomery Jr., J. E. Peralta, F. Ogliaro, M. Bearpark, J. J. Heyd, E. Brothers, K. N. Kudin, V. N. Staroverov, R. Kobayashi, J. Normand, K. Raghavachari, A. Rendell, J. C. Burant, S. S. Iyengar, J. Tomasi, M. Cossi, N. Rega, J. M. Millam, M. Klene, J. E. Knox, J. B. Cross, V. Bakken, C. Adamo, J. Jaramillo, R. Gomperts, R. E. Stratmann, O. Yazyev, A. J. Austin, R. Cammi, C. Pomelli, J. W. Ochterski, R. L. Martin, K. Morokuma, V. G. Zakrzewski, G. A. Voth, P. Salvador, J. J. Dannenberg, S. Dapprich, A. D. Daniels, Ö. Farkas, J. B. Foresman, J. V. Ortiz, J. Cioslowski, D. J. Fox, *Gaussian 09, Revision D.01* (Gaussian Inc., 2009).
34. N. S. Mills, K. B. Llagostera, Summation of nucleus independent chemical shifts as a measure of aromaticity. *J. Org. Chem.* **72**, 9163–9169 (2007).
35. Z. Chen, C. S. Wannere, C. Corminboeuf, R. Puchta, P. v. R. Schleyer, Nucleus-independent chemical shifts (NICS) as an aromaticity criterion. *Chem. Rev.* **105**, 3842–3888 (2005).
36. J. P. Perdew, K. Burke, M. Ernzerhof, Generalized gradient approximation made simple. *Phys. Rev. Lett.* **77**, 3865–3868 (1996).
37. J. M. Soler, E. Artacho, J. D. Gale, A. García, J. Junquera, P. Ordejón, D. Sánchez-Portal, The SIESTA method for *ab initio* order-*N* materials simulation. *J. Phys. Condens. Matter* **14**, 2745–2779 (2002).
38. J. B. Neaton, M. S. Hybertsen, S. G. Louie, Renormalization of molecular electronic levels at metal-molecule interfaces. *Phys. Rev. Lett.* **97**, 216405 (2006).
39. S. Refaely-Abramson, S. Sharifzadeh, N. Govind, J. Autschbach, J. B. Neaton, R. Baer, L. Kronik, Quasiparticle spectra from a nonempirical optimally tuned range-separated hybrid density functional. *Phys. Rev. Lett.* **109**, 226405 (2012).
40. D. A. Egger, Z.-F. Liu, J. B. Neaton, L. Kronik, Reliable energy level alignment at physisorbed molecule–metal interfaces from density functional theory. *Nano Lett.* **15**, 2448–2455 (2015).

Acknowledgments

Funding: The experimental work was supported primarily by the NSF (award no. DMR-1507440). The computational work was supported by the Molecular Foundry and by the Materials Sciences and Engineering Division (Theory FWP), U.S. Department of Energy, Office of Basic Energy Sciences (contract no. DE-AC02-05CH11231). Portions of the computation work were performed at the National Energy Research Scientific Computing Center. J.Z.L. would like to thank the Agency for Science, Technology and Research (A*STAR) Graduate Academy in Singapore for a graduate fellowship. **Author contributions:** The project was planned by L.M.C. and L.V. **TBTP** was synthesized and characterized by L.Z. and X.Y. Electrochemistry and UV-vis spectroscopy measurements were conducted by X.Y. and J.Z.L. STM-BJ measurements were conducted by L.V., Y.Z., and J.C. The data analysis was performed by L.V., L.M.C., Y.Z., and X.Y. The calculations were carried out by Z.-F.L. and J.B.N. The manuscript was prepared by J.B.N., L.M.C., L.V., X.Y., Y.Z., and Z.-F.L. **Competing interests:** The authors declare that they have no competing interests. **Data and materials availability:** All data needed to evaluate the conclusions in the paper are present in the paper and/or the Supplementary Materials. Additional data related to this paper may be requested from the authors.

Submitted 1 July 2017
Accepted 5 October 2017
Published 27 October 2017
10.1126/sciadv.aao2615

Citation: X. Yin, Y. Zang, L. Zhu, J. Z. Low, Z.-F. Liu, J. Cui, J. B. Neaton, L. Venkataraman, L. M. Campos, A reversible single-molecule switch based on activated antiaromaticity. *Sci. Adv.* **3**, eaao2615 (2017).

A reversible single-molecule switch based on activated antiaromaticity

Xiaodong Yin, Yaping Zang, Liangliang Zhu, Jonathan Z. Low, Zhen-Fei Liu, Jing Cui, Jeffrey B. Neaton, Latha Venkataraman and Luis M. Campos

Sci Adv **3** (10), eaao2615.
DOI: 10.1126/sciadv.aao2615